

# **DesignCon 2011**

## Stack-up and routing optimization by understanding micro-scale PCB effects

Gerardo Romo L., CST of America

Chudy Nwachukwu, Isola Group

Reydezel Torres-Torres, INAOE

Seung-Won Baek, CST of America

Martin Schauer, CST of America

## **Abstract**

The high-frequency content of state-of-the-art digital signals acts like a magnifying glass for microscale PCB effects like glass weave and copper surface roughness. In this paper, we present an experimental, numerical, and analytical investigation of the important role that these effects play in defining the characteristic impedance of interconnects, the associated attenuation and phase constant, as well as the appearance of resonances in the insertion and return loss. By means of 3D EM simulations, macromodels are developed and correlated to measurements up to 50 GHz using a test vehicle designed using different prepregs, laminates and copper foils. As a result, recommendations and guidelines are provided for proper material selection and trace routing that mitigate such effects.

Summary: PCB laminates are inhomogeneous structures constructed from multiple dielectric and metal layers. Thus, the anisotropic nature of PCBs introduces a variation of the dielectric characteristics of the substrate with position and may also originate resonances that considerably degrade the performance of interconnects. Despite this, it is a common practice for design engineers to solely rely on vendor published  $\epsilon$  and  $\tan\delta$  parameters obtained by a Bereskin and/or Stripline-resonator technique applied to smooth resin cast of homogenous material. Similarly, the properties of metal layers are typically characterized by bulk properties; at best, modified based on the model developed by Hammerstad and Jensen to account for the increase on the attenuation due to copper roughness. However, as communication speeds continue to rise, it becomes imperative to analyze the impact of micro-scale effects not only on the attenuation constant, but also on the phase constant and the characteristic impedance of the interconnects so that accurate representations can be achieved for reliable circuit design.

In this paper, we study these micro-scale effects in detail. In particular, we analyze the dependence of the electrical properties of interconnects with respect to their position on the weave as well as the effects that result from the periodicity of the fiber glass bundles, which can give rise to resonances. Furthermore, we discuss the mechanisms that produce such resonances and propose an analytical equation for their prediction, validated by 3D electromagnetic simulations and measurements. For this purpose, a 3D fabric weave model based on actual prepreg layer measurements is created and simulated using an EM simulator. A PCB test vehicle was fabricated with sets of traces running at various angles. The predicted, simulated, and measured resonances are shown to be in excellent agreement.

The focus of our investigation of copper roughness is not only on the additional attenuation introduced by the roughness, but also on the additional time delay, which can be directly extracted from our time-domain simulations. The investigation starts with the common approach where the copper surface bumps are assumed to be periodic. A parameterized model is developed which takes given surface statistics as input. The statistical data to generate such models are taken directly from optical profile meter measurements of copper foils. Bear in mind, however, that the large aspect ratio between the roughness feature size and the overall interconnect length makes the use of these 3D models currently unfeasible. For this reason, we propose a computationally inexpensive

macromodel based on a frequency-dependent surface impedance model. After the models are developed, we use them to predict the effects of copper roughness on signal propagation and to characterize the copper foil by simulation. Our models are then correlated to existing models and measurements.

For the experimental validation of the modeling results presented in this paper, we determine the complex propagation constant ( $\gamma$ ) and characteristic impedance ( $Z_c$ ) of various high speed test lines. In our experiments we determine  $\gamma$  and  $Z_c$  from line-line measurements, which is desirable for a more accurate and systematic characterization of the micro-scale effects on high-speed interconnects. Finally, as a result of our micro-scale investigations of PCBs, we provide guidelines and recommendations for material selection, stack-up optimization and trace routing not only for taking these effects into consideration but also for mitigating them as much as possible.

## **Authors Biography**

Gerardo Romo obtained the Ph.D. degree in electrical engineering from Carleton University, Ottawa, ON, in 2005. From 2005 to 2008, he was a Sr. Hardware Engineer at the Systems Research Center of Intel Mexico, working on R&D of high-speed interconnects and electronic packages. His main research focused on exploring alternative technologies for high-speed interconnects such as Substrate Integrated Waveguides and non-linear Transmission lines. In 2009, he joined CST of America as an Application Engineer with emphasis on signal and power integrity applications.

Chudy Nwachukwu is an Electrical Application Development Engineer at Isola Group, responsible for designing test vehicles and engineering applications to meet the requirements of OEMs in the high speed digital market. He obtained his bachelor's degree in Mathematics and Computer Science at Southwest Minnesota State University, Marshall MN in 2006. He completed his M.S in Electrical Engineering at Saint Cloud State University, Saint Cloud MN in 2009 and published his graduate Thesis on Design optimization of components in High Speed PCBs. He worked for Force10 Networks in San Jose, CA from 2007 - 2009 specializing in signal integrity, 3D modeling and Electromagnetic analysis of line card and backplane channels.

Reydezel Torres-Torres is a senior researcher in the Microwave Research Group of the National Institute for Research in Astrophysics, Optics, and Electronics (INAOE) in Mexico. He has authored 30 journal and conference papers and directed one PhD. and 6 M.S. theses, all in high-frequency characterization and modeling of materials, interconnects, and devices for microwave applications. He received his PhD from INAOE and has worked for Intel in Mexico and IMEC in Belgium.

Seung-Won Baek is an application engineer at CST of America. He has previously worked for LG Electronics, KMW(Korea MicroWave), and KBSI(Korea Basic Science Institute). His previous experiences include a variety of vacuum tubes, appliances and RF components designs. He holds fourteen International Patents and sixteen Domestic Patents on vacuum tubes.

Martin Schauer received the Dipl.-Ing. degree in Electrical Engineering from the Technische Universität Darmstadt in 1999. In the same year, he joined the Computational Electromagnetics Laboratory (TEMF) for Theory of Electromagnetic Fields, where he earned his Ph.D. in 2005. Since 1999 he is with Computer Simulation Technology (CST), where he developed 3D electromagnetic simulation software until 2005. Currently he is working as a principal application engineer and technical key account manager for CST of America in the San Francisco Bay area. His main interests are numerical methods and their application towards low and high frequency electromagnetic problems.

# 1 Introduction

In selecting a glass style for Printed Circuit Board (PCB) construction, a number of variables must be taken into consideration. The glass weave pattern, thread count and yarn thickness are the main parameters that will determine the style of glass to be incorporated to meet the demands of the application. PCB laminates are manufactured by impregnating and strengthening a woven fiberglass fabric with epoxy resin. These laminates are generally available in various constructions (different glass styles of varying thickness bound together with resin in different proportions) to achieve a desired thickness. See Figure 1 below for examples of weaves with varying counts of warp yarn versus weft yarn<sup>1</sup>. Two traditional glass styles (left) are depicted in a spread weave pattern (right).

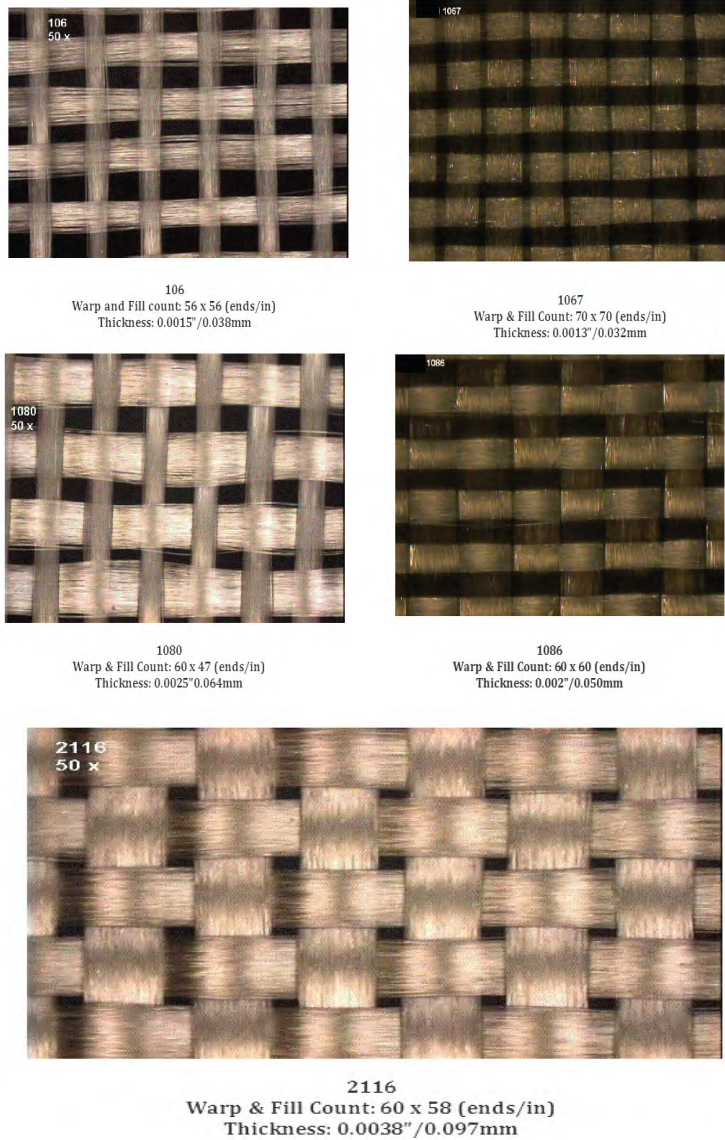


**Figure 1:** Depiction of commonly used glass weaves.

<sup>1</sup> Pictures courtesy of Isola R&D laboratories

E-glass, S-glass and NE-glass fabric are commercially available in thicknesses ranging from 1mil to 60mils and resin impregnation percentages required for manufacturing laminate and prepreg range from 41% to 75%. Specialized applications might require a percentage outside of this range, but this is uncommon and difficult to process. A simple but commonly used equation for calculating the resulting permittivity of a composite material is:

$$\epsilon_{r_{composite}} = \epsilon_{r_{resin}} \times \text{Percentage Resin} + \epsilon_{r_{glass}} \times (1 - \text{Percentage Resin})$$

The mechanical and electrical properties of the composite material typically depend on the amount of impregnation, and this is affected by the density of the weave and balanced/unbalanced count of the warp and weft yarns. Proper selection of dielectric material to minimize losses in PCBs requires knowledge of the electrical characteristics of the resulting resin-glass composite.

### Composite Material

Laminate manufacturers typically specify the electrical properties of their resin-systems as it relates to the construction type. See Table 1 below for an example of laminate constructions of a high performance resin-system used in the fabrication of our test vehicle described in a later section.

I - Tera Global Standard Constructions					
Core Thickness (inches)	Core Thickness (mm)	Standard	Resin %	Dk @ 10GHz	Df @10GHz
0.0025	0.064	1 x 1067	70 %	3.10	0.0030
0.0030	0.076	1 x 1067	75 %	3.00	0.0030
0.0033	0.0825	1 x 1086	62 %	3.25	0.0032
0.0035	0.0890	1 x 1086	64 %	3.20	0.0032
0.0040	0.1000	1 x 1080	72 %	3.00	0.0030
0.0040	0.1000	1 x 1086	68 %	3.15	0.0031
0.0040	0.1000	1 x 3070	50 %	3.45	0.0036
0.0045	0.0114	1 x 1086	71 %	3.05	0.0030
0.0045	0.1130	1 x 3313	60 %	3.25	0.0032
0.0050	0.1250	1 x 2116	54 %	3.38	0.0035
0.0050	0.1250	1 x 3313	62 %	3.25	0.0032
0.0050	0.1250	2 x 1067	70 %	3.10	0.0030
0.0060	0.1500	2 x 1067	75 %	3.00	0.0030
0.0066	0.1650	2 x 1086	62 %	3.25	0.0032
0.0070	0.1750	2 x 1080	68%	3.15	0.0031
0.0080	0.2000	2 x 3070	50 %	3.45	0.0036
0.0080	0.2000	2 x 1080	72 %	3.00	0.0030
0.0100	0.2500	2 x 3313	62 %	3.25	0.0032
0.0100	0.2500	2 x 2116	54 %	3.38	0.0035
0.0100	0.2500	2 x 3070/ 1086	50 %	3.45	0.0036
0.0120	0.3000	3 x 1080	72 %	3.00	0.0030
0.0133	0.3330	2 x 2116 / 1 x 1086	56 %	3.33	0.0033
0.0140	0.3500	2 x 2116 / 1 x 1080	60 %	3.25	0.0032
0.0160	0.4000	4 x 1080	72 %	3.00	0.0030
0.0166	0.4150	2 x 2116 / 2 x 1086	57 %	3.33	0.0033
0.0180	0.4500	2 x 2116/ 2 x 1080	62 %	3.25	0.0032

Table 1: I-Tera Standard construction<sup>2</sup>.

<sup>2</sup> Constructions provided courtesy of Isola Laminates

## Micro-scale Fiber Weave Effects

Despite the inhomogeneous composition of PCB laminates discussed in the previous section, they have been treated as homogeneous for many years. However, as data rates continue to increase, it has become evident [1,2], that the local variations of the material properties can no longer be neglected because they play an important role in the performance of high speed interconnects.

In [1], it was found that the local variations of the dielectrics can lead to unbalanced lines on high speed buses because it is likely that some lines will lie on top of the fiberglass bundles while others will lie in-between the bundles. In [2], it was found that the periodic loading of interconnects introduced by the fiberglass bundles can lead to resonances in the insertion and return loss characteristics. In the same work, comprehensive numerical and graphical studies of resonances were performed. In particular, the roles of the pitch between fiberglass bundles and trace angle (with respect to the bundles) were studied. However, the results were presented in a series of surface plots which make the extraction of data somewhat cumbersome.

In this paper, we revisit the effect of periodic fiberglass loading on traces running at an arbitrary angle with respect to the weave. It is well established that periodic loading results in a fundamental resonance at a frequency whose associated half-wavelength equals the separation between the periodic loads. Through a careful analysis of a fiber weave model, we find an analytical expression that allows us to predict the resonance frequency as a function of the material properties (such as pitch and effective permittivity), and the angle between the trace and the fiberglass bundles. As it will be demonstrated, the derived expression is very accurate in predicting the resonance frequency for arbitrary angles.

For the derivation, consider the trace of Figure 2 which is running at an angle  $\Phi$  with respect to the weft of the weave. Note that in the following analysis, we randomly denoted the vertical and horizontal fiberglass bundles as the warp and weft yarns respectively, but the same analysis holds for the opposite scenario. As the figure shows, the trace is periodically loaded by both the weft and the warp yarns. Also, note that for angles larger than  $45^\circ$ , the weft and warp interchange roles with respect to the trace, therefore we only need to concern ourselves with angles between  $0^\circ$  and  $45^\circ$  but the analysis is valid for any arbitrary angle.

Although it is true that the combination of weft and warp loading results in some complex periodicity patterns, the two effects can be analyzed separately. As Figure 2 shows, the period of the warp is very small (in the range of the fiberglass bundle pitch) regardless of the angle. More strictly, this is true for angles between  $0^\circ$  and  $45^\circ$  which is the range before the weft and warp interchange roles with respect to the trace. Because of the small spatial period of the warp-induced loading, the corresponding resonances would be too far out in frequency to be of importance for state-of-the-art high speed interconnects. Thus, their effect can, for now, be neglected.

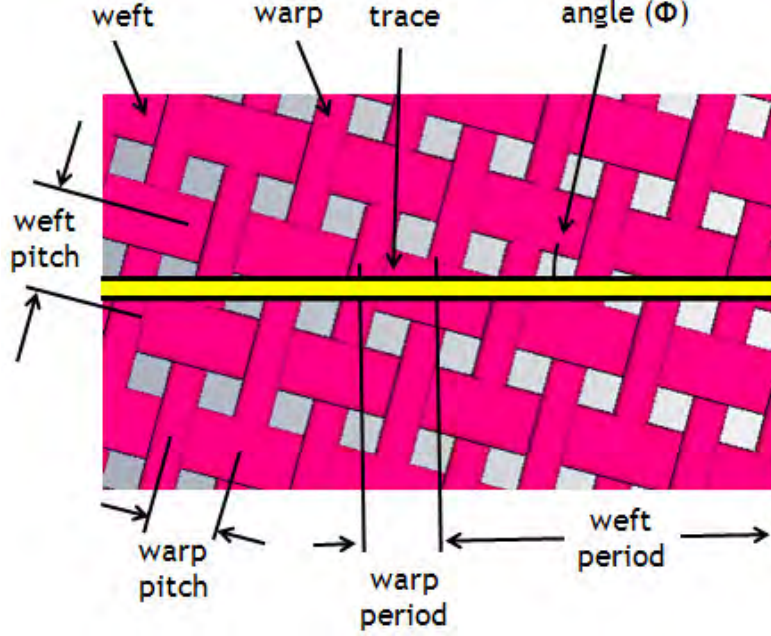


**Figure 2:** Definitions used for the analysis of the fiber weave effect.

The same analysis of the periodic effect induced by the weft reveals a very different scenario. As the figure shows, the periodic loading of the weft occurs over longer spatial periods. As it will be demonstrated, this type of periodic loading is actually responsible for the resonances which fall within the operating range of state-of-the-art high speed interconnects. In order to obtain an expression for predicting such resonances, we first need to determine the spatial weft period. From the figure, the weft period can easily be obtained from trigonometric expressions. It is given by:

$$weft\ period = \sqrt{pitch^2 \left( \frac{1}{[\tan(\Phi)]^2} + 1 \right)} \quad (1)$$

and it follows that the associated resonance frequency ( $f_{res}$ ) is given by:

$$f_{res} = \frac{c}{2 \times \sqrt{\epsilon_{eff} pitch^2 \left( \frac{1}{[\tan(\Phi)]^2} + 1 \right)}} \quad (2)$$

In the Equation 2,  $c$  is the speed of light in vacuum,  $\epsilon_{eff}$  is the effective permittivity of the dielectric, pitch is the “weft pitch” in the Figure 2, and  $\Phi$  is the angle between the trace and the weft bundles also as shown in the figure.

Figure 3 (Left) shows the resonance frequencies for various pitches and trace-to-weft angles as predicted by Equation 2. As the figure indicates, the critical routing angles heavily depend on the weft pitch and the maximum frequency of interest. For example, taking the 1080 material as a reference, one can see that routing angles larger than  $20^\circ$  would prevent the appearance of resonances below 50 GHz. Furthermore, we can generalize this result to other materials by stating that routing angles larger than  $20^\circ$  should be used in order to prevent the appearance of fiber-weave-induced resonances

below 40 GHz. This is, perhaps, a safe assumption given the current operating frequencies of high speed interconnects. In this regard, the figure shows that routing angles smaller than  $10^\circ$  are potentially the most prone to originate resonances. However, this assertion requires a more careful consideration because the appearance of resonances is also dependant on other factors as discussed next.

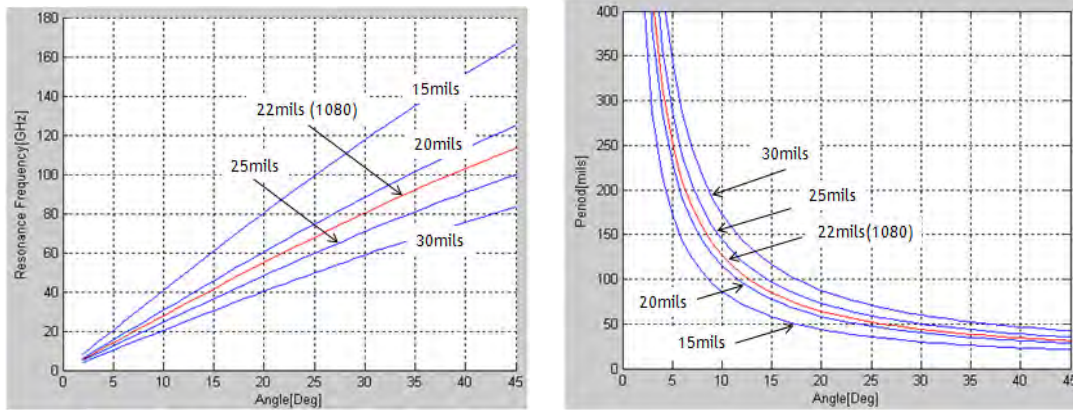


**Figure 3:** (Left) Resonance frequencies for different pitches and trace-to-weft angles predicted by Equation 2.  $\epsilon_{eff}=2.8$  was used. Right: weft period for different pitches and trace-to-weft angles as predicted by Equation 1.

### Fiber Weave Effects Determining the Magnitude of Resonance

The magnitude of the resonance peak (or dip) depends on two factors: the **number** and the **size** of the periodic loads. In a practical application, the number of periodic loads is given by the number of crosses (per unit length) between the trace and the weft yarn. That is, for fixed material properties, the magnitude of the resonance will depend on the number of weft periods spanning the trace. The more weft periods per unit length of trace, the higher the magnitude of the resonance. Thus, for a given trace length, the mitigation of fiber-weave-induced resonances is favored for small routing angles because the weft period becomes increasingly large compared with the trace length.

Figure 3 (right) shows the weft period for various pitches and trace-to-weft angles as predicted by Equation 1. As the figure shows, for angles close to zero ( $\Phi < 5^\circ$ ), the weft period becomes increasingly large ( $>400$ mils). Note that in the limit ( $\Phi = 0^\circ$ ), the weft period becomes infinite (the weft bundles and trace are parallel to each other) and the only potential resonance can be generated by the warp loading. Thus, for small angles and typical interconnect lengths, there will be a very small number of crosses between the trace and the weft. Under these conditions, the magnitude of the resonance will be very small or might not appear at all. The number of periods that a given interconnect can tolerate before a potential resonance becomes critical for a given design needs to be determined through simulation.

From the previous analysis, we can see that the smallest routing angle with potential to generate resonances is determined by the longest interconnect of interest. A corollary of this assertion is that for fixed routing angles, short interconnects are more robust to resonances than long interconnects. Thus, particular care must be paid when designing long busses, for example, on backplanes.

As previously mentioned, the second factor that determines the magnitude of the fiber-weave-induced resonances is the size of the periodic load which is determined by the dielectric contrast between the fiberglass bundles and the voids in-between. Note that the voids are, for the most part, filled with resin. In general, for a fixed weft period, the larger the dielectric contrast between the fiberglass bundles and the voids, the larger the magnitude of the resonance frequency. Note that this condition is more strongly satisfied by materials with sparse weave such as 106 and 1080. As a matter of fact, it will be demonstrated in later sections that materials with a very dense weave such as 2116, can potentially suppress the appearance of resonances due to their intrinsic weak periodic loading. For a given interconnect design, whether the intrinsic dielectric contrast of the chosen material can lead to critical resonances or not, should be determined through simulation.

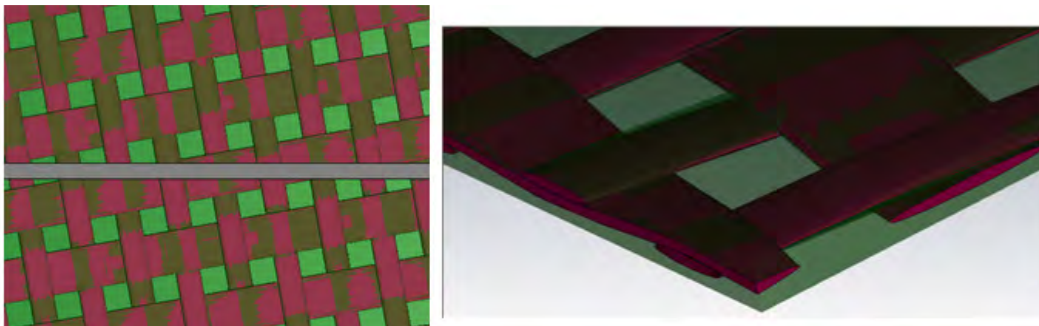
### Simulations of Fiber Weave Effect

In this section, we investigate the fiber weave effect by means of three dimensional simulations. For this purpose, CST MICROWAVE STUDIO®, a full wave electromagnetic simulator, is used. Firstly, we intend to validate the accuracy of the equation derived in the previous section. Second, we demonstrate that despite the prediction capability provided by Equation 2, full wave simulations are still required to determine the magnitude of the resulting resonance from the number and size of the periodic loads. For this purpose, two different glass styles (1080 and 2116) of dielectric material are simulated. These choices are made because 1080 is a highly inhomogeneous material (due to its sparse weave) and resonances are likely to appear. In contrast, 2116 is a more homogeneous material and resonances are less likely to occur. The 1080 and 2116 weaves are shown in Figure 1 for comparison. Table 2 shows the details of the performed simulations:

	<b>1080</b>	<b>2116</b>
Weft pitch (mils)	22.00	25.92
Warp pitch (mils)	15.92	23.83
Fiberglass thickness (mils)	2.1	3.6
Total pre-preg thickness (mils)	3.8	5.6
Resin ( $\epsilon/\text{TanD}$ )	3.3/0.003	3.3/0.0034
Fiberglass ( $\epsilon/\text{TanD}$ )	4.8/0.003	4.8/0.0034
Trace to weft angle	0°, 7°, 10°, 15°	0°, 7°, 10°, 15°
Trace (width/thickness/length) mils	9.4/0.7/4000	13/0.7/4000

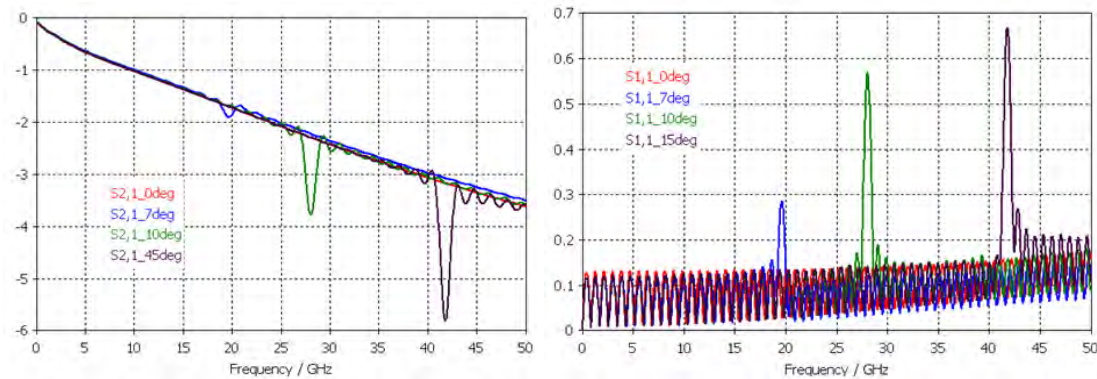
**Table 2:** Details of simulated structures.

Figure 4 shows some details of the simulated three dimensional models.



**Figure 4:** Details of the simulated three dimensional models (1080).

Figure 5 shows the simulated insertion and return loss of the 1080 material. The figures show very interesting results. First of all, it is observed that, except for  $0^\circ$ , the resonance is present for all simulated angles. Notice that a resonance for  $0^\circ$  also occurs, but outside the simulated frequency range because in this case it is related to the (small) spatial period of the warp-induced loading. The resonances are a result of the strong local material variations of the highly inhomogeneous 1080 dielectric. Second, the predicted resonances by Equation 2 are in excellent agreement with the simulation results. See Table 4. This validates the fact that the equation derived in the previous section can predict the fiber-weave-induced resonances very accurately. Third, the figures corroborate the fact that the magnitude of the resonances is proportional to the number of weft periods per unit length. As expected, the resonance is stronger for larger angles because the number of periods per unit length increases. With the help of Equation 1, the number of periods per inch are: 5.54, 7.89 and 11.76 for  $7^\circ$ ,  $10^\circ$  and  $15^\circ$  respectively.



**Figure 5:** Simulated insertion (left) and return loss (right) of the 1080 material.

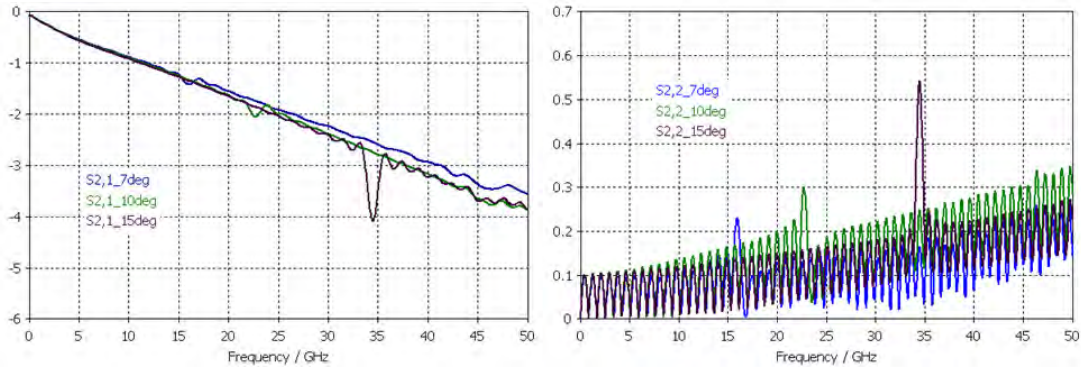


**Figure 6:** Simulated insertion (left) and return loss (right) of the 2116 material.

Figure 6 shows the simulated insertion and return loss for the 2116 material. As the figures show, the simulation results predict weaker resonances for this case. As previously discussed, this is a result of the denser weave comprising the 2116 material. Thus, the dense weave leads to weaker local material variations which mitigate the appearance of fiber-wave-induced resonances for this type of material. Notice that despite the weak resonances, the frequencies are also in perfect agreement with the predictions by Equation 2.

In addition to the appearance of resonances, the fiber weave effect also manifests itself by changing the electrical characteristics of high speed interconnects based on their specific location on the (weave) board. In order to get a feel for the magnitude of this

effect, we simulated and extracted the characteristic impedance and  $\epsilon_{eff}$  permittivity for various lines lying on different locations on the board with respect to the weave ( $\Phi=0^\circ$ ). Because we are looking for the worst case scenario, the 1080 material was used for the simulations. The results are shown in Figure 7.

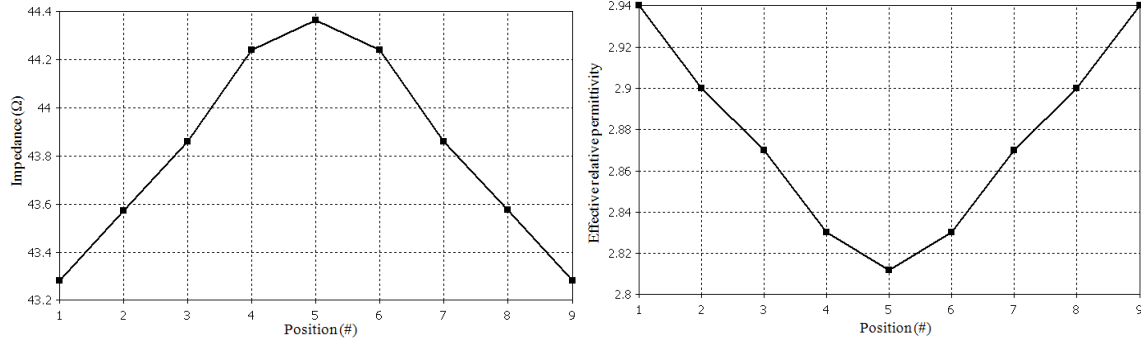


**Figure 7:** Left: Characteristic impedance and Right:  $\epsilon_{eff}$  for various lines lying on different locations on the board with respect to the weave ( $\Phi=0^\circ$ ). Positions 1 and 9 correspond to trace over bundles.

Our simulations show only a slight variation of the trace’s characteristic impedance and effective permittivity as a function of different positions on the weave. As will be seen later, this is in agreement with our experimental results.

## Surface Roughness Modeling

Another important micro-scale effect on PCBs is copper surface roughness. Increasing data rates and recent developments on low loss substrates make this effect more important nowadays. Early work on this topic was mostly in combination with scattering of rough surfaces for radar or particle accelerators, but in the recent years, an increased number of publications focused on understanding the effect of surface roughness on PCBs for high speed data transmission.

This chapter is divided in the following topics: First, we review the information available in copper foil datasheets and compare it to a surface measurement for standard and low profile copper foils. Then we start with a simple modeling of surface roughness as a periodic structure with a sinusoidal profile. We finally describe how this information can be used in a macroscopic material definition using a frequency-dependent surface impedance model.

## Copper Foil Datasheet and Surface Measurement

In order to incorporate surface roughness into simulation and modeling we first would like to understand, what information is typically available to the design engineer. Figure 8 shows a typical cross-section of a copper trace. It should be noted that copper foils usually have two sides, an untreated one and a treated one. The treated side is rougher for better adhesion of the foil to the laminate. It can also be noted that surface roughness is a random, statistical effect. As such the following definitions for the center-line average (CLA)  $R_a$  and the RMS roughness  $R_q$  are standardized [3]:

$$R_a = \frac{1}{L} \int_0^L |z(x)| dx$$

$$R_q = \sqrt{\frac{1}{L} \int_0^L z^2(x) dx}$$

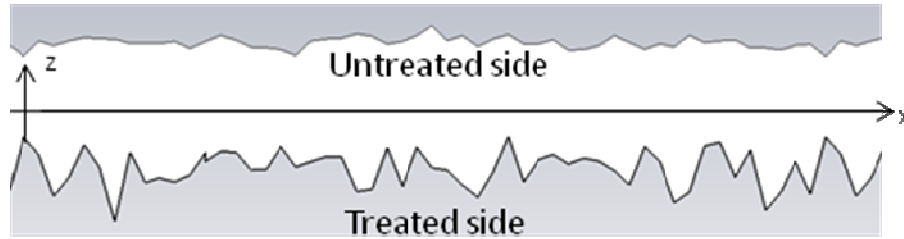


**Figure 8:** 1D example of a rough copper profile.

In addition, datasheets often provide a value of  $R_z$  which is the mean of five roughness depths over successive samples.

For this paper, an optical profile-meter measurement of the treated side of two copper foils was performed. These data allow us to analyze the statistics of the copper foils. Figure 9 shows a 100x100 sample of the data generated as output. It can be easily observed that the deviation of peaks and valleys for low-profile copper is much less than that for standard foil. Since typically  $R_a$  is given in the datasheet, but  $R_q$  is statistically a more accurate description, we are particularly interested in the ratio of  $R_a/R_q$ . For a sinusoidal surface  $R_a/R_q$  is  $\sim 0.9$  and for a Gaussian height distribution  $R_a/R_q$  is  $\sim 0.8$  [3].

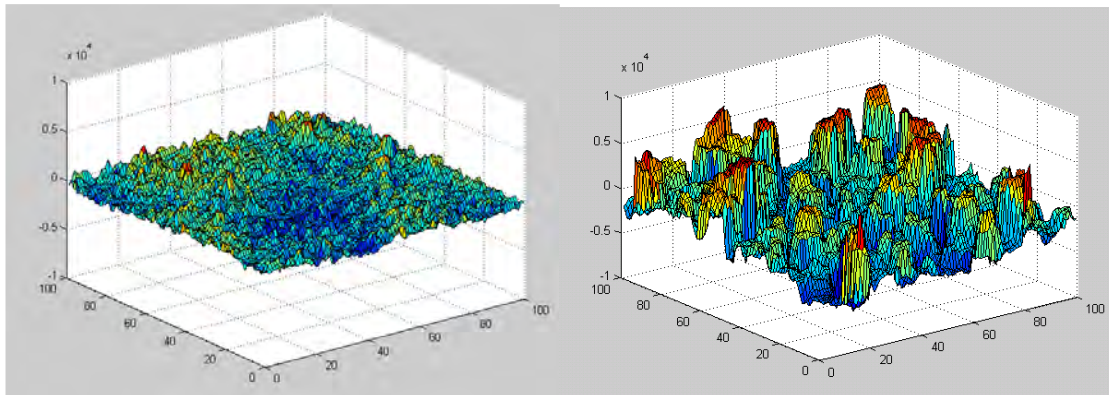


**Figure 9:** 100x100 surface sample data for low-profile copper (left) and standard copper (right).

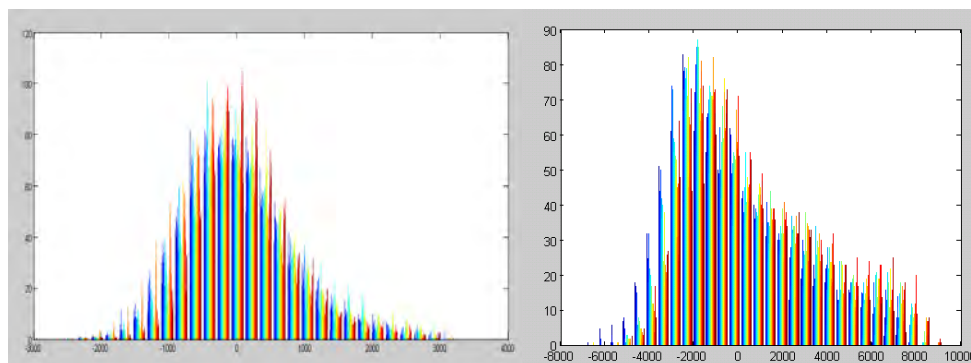


**Figure 10:** Histogram of the surface deviation from flat copper for low-profile copper (left) and standard copper (right) using 30 bins.

Figure 10 shows a histogram of the surface deviation from average for the two Cu profiles. The plot used 30 equally distributed bins and shows the number of discrete

samples which fall in each bin. It is notable that the low-profile copper has a statistical distribution close to a Gaussian shape, with only slight skew. The standard copper, however, has a larger skew towards peaks. In Table 3 the surface statistics are listed.

	Low-profile copper	Standard copper
Range (maximum-minimum)/nm	6208	15979
$R_q$ / nm	666.0129	2553.4
$R_a$ / nm	531.6802	2099.4
$R_a / R_q$	0.7983	0.8222

**Table 3:** Summary of surface statistics for the measured treated side.

It is notable that the *rms* roughness  $R_q$  for standard copper is around four times larger than that of low profile copper. Both show that despite the deviation from a Gaussian distribution, the values are not too far from the assumption of 0.8 for  $R_a / R_q$

### Modeling Surface Roughness as a Periodic Effect

As a next step we want to investigate the effect of *rms* roughness as well as the spatial periodicity on the insertion loss and phase delay of transmission lines [4]. The first studies performed are parametric sweeps over the amplitude ( $R_q$ ) as well as the spatial frequency  $f_s$ , Figure 11.

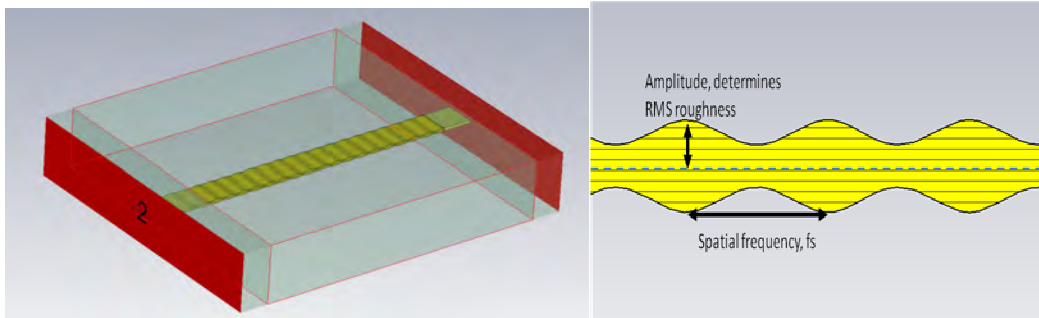


**Figure 11:** The periodic model and its parameters.

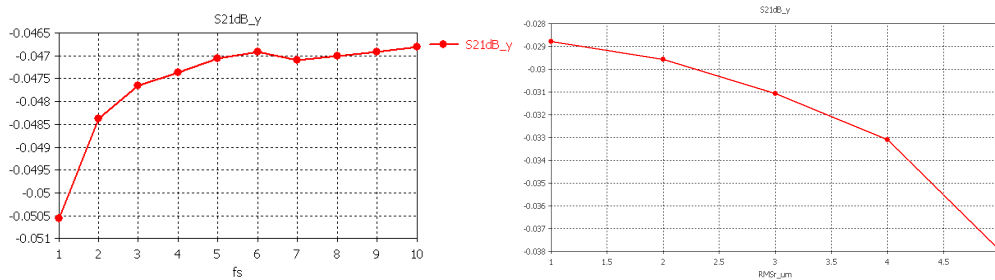


**Figure 12:** Insertion loss at 50 GHz versus spatial frequency ( $f_s$ ) on the left, and versus *rms* roughness in  $\mu\text{m}$  on the right.

The results for the spatial frequency in Figure 12 show clearly a systematic variation with the spatial frequency ( $f_s$ ). The higher the spatial frequency, the higher the loss. It should be mentioned that all these models have the same *rms* roughness. This suggests that depending on the microstructure of the roughness, different loss values can be expected

even for the same *rms* value. In Figure 13, the insertion loss at 50 GHz for a variation of the *rms* roughness show the expected result that rougher surfaces exhibit higher loss.

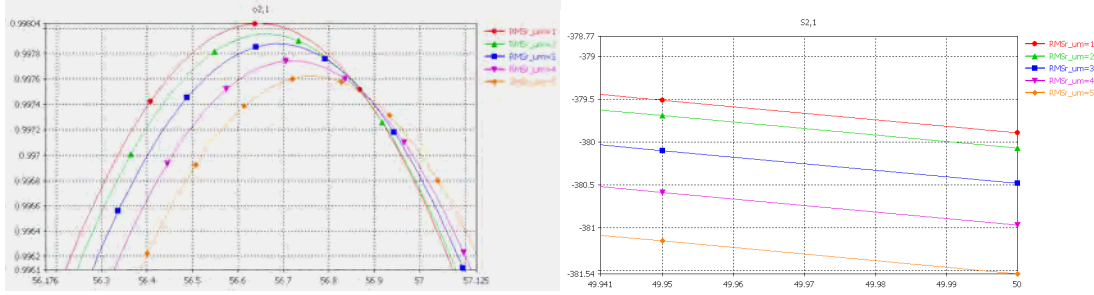


**Figure 13:** The pulse response when the pulse maximum is reached (left), and the corresponding phase delay at 50 GHz versus *rms* roughness (right).

In addition to the amplitude variations, also the time delay in the full wave 3D time domain simulation is monitored, as well as the phase of the corresponding S-parameters. We notice that when we zoom into the maximum of the received voltage pulse, higher *rms* values of course result in a lower amplitude, but it can also be observed that the maximum occurs at later times. In the frequency domain this translates to a higher phase shift at 50GHz, as we increase the *rms* roughness.

### Surface Impedance Model

As the previous study has shown, modeling a detailed periodic or random surface over realistic transmission line length (1-10 in) can be computationally expensive. A better approach would be to transition from the micro-scale to a macroscopic model, which still captures the most important properties. Such a model was developed by Hammerstad and Jensen. According to their studies, the additional surface resistance for rough surfaces can be described by [5],

$$R_s(\Delta) = R_s(0) \left( 1 + \frac{2}{\pi} \arctan \left( 1.4 \left( \frac{R_q}{\delta} \right)^2 \right) \right),$$

with the surface resistance of the flat metal  $R_s(0)$ , the *rms* roughness  $R_q$  and the skin depth  $\delta$ . The Hammerstad and Jensen surface resistance can be implemented into numerical full-wave 3D solvers (time- and frequency domain) as a frequency dependent modification of the general surface impedance model [6]. Rautio described in detail how the surface impedance  $Z_s$  can be implemented at frequencies well above the frequency at which the skin effect starts becoming apparent; for a given conductivity  $\sigma$  and permeability  $\mu$ ,  $Z_s$  is expressed as [7]:

$$Z_s = (1 + j) R_{RF} \sqrt{f}$$

$$R_{RF} = \sqrt{\frac{\pi \mu}{\sigma}}$$

It is worth to mention that this formula will create a surface impedance with equal real and imaginary parts. As a result, an increased surface resistance from copper roughness will also impact the equivalent capacitance/inductance and cause some time delay in the transmission. In order to investigate this effect and to get a better understanding of this

model, a simulation experiment of a 40 mil microstrip line with different copper finishes is carried out.

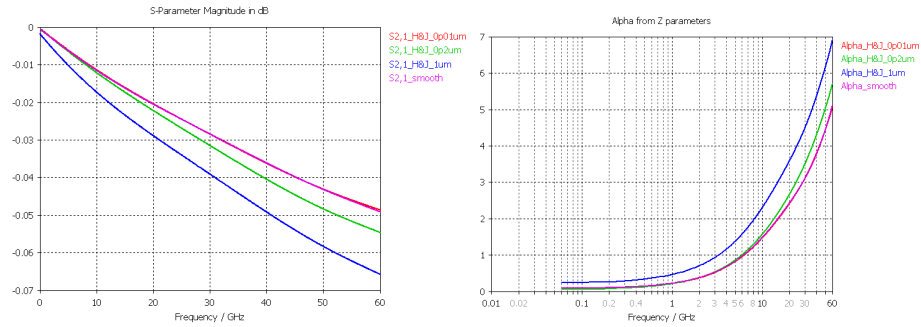


**Figure 14:** Insertion loss versus frequency for different copper models (left) and loss coefficient  $\alpha$  versus frequency (right).

Figure 14 shows that for a very small *rms* roughness  $R_q$ , the results converge and coincide with those of flat copper. When the roughness is increased, the loss also increases, up to a certain point, where it reaches saturation for this particular frequency.

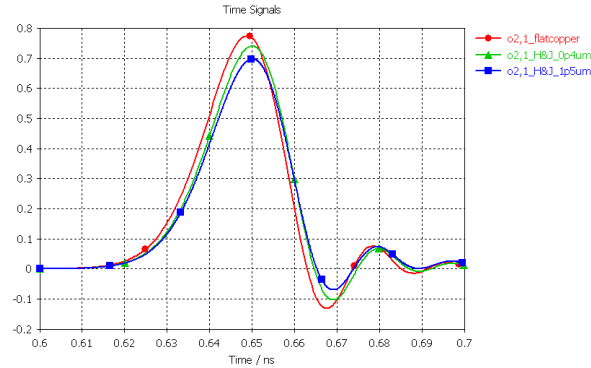


**Figure 15:** Output voltage for a Gaussian pulse at the end of a 4-in microstrip transmission line. The copper is modeled as flat (red circle), using the Hammerstad and Jensen model with  $R_q = 0.4 \mu\text{m}$  (green triangle) and  $R_q = 1.5 \mu\text{m}$  (blue square).

A similar experiment was carried out over a 4-in microstrip line, see Figure 15. We can clearly observe the increased attenuation if rougher copper is used as well as a time delay over rough copper compared to flat copper.

## Test Vehicle Design

Isola Group, CST and INAOE collaborated to design an experimental test vehicle to investigate micro-scale effects of laminate weave and copper roughness. The material properties of I-Tera were obtained from isoStack<sup>TM</sup>, and the 8-layer stack up was designed using the web-based design application [8]. The details of the stack-up are shown in Figure 16. The design requirements were as follows:

- I-Tera material, 50  $\Omega$  SE microstrip design routed on 1080 and 2116 weave based resin-system.
- 1/2-Oz smooth low profile VLP copper [9] and 1/2-Oz standard TWS copper [10] routed on top and bottom of PCB.

## Test Structures

Multiple trace geometries were implemented on this board to investigate the effects of the laminate weave on impedance and insertion loss parameters. The test vehicle and structures are shown in Figure 17. Probe launch pads at 250 $\mu$ m pitch were built into test structures to ensure consistent, repeatable measurements of S-parameters at frequency ranges in excess of 40 GHz. The board was fabricated by R&D circuits, NJ and the measurements were performed at INAOE in Puebla, Mexico.

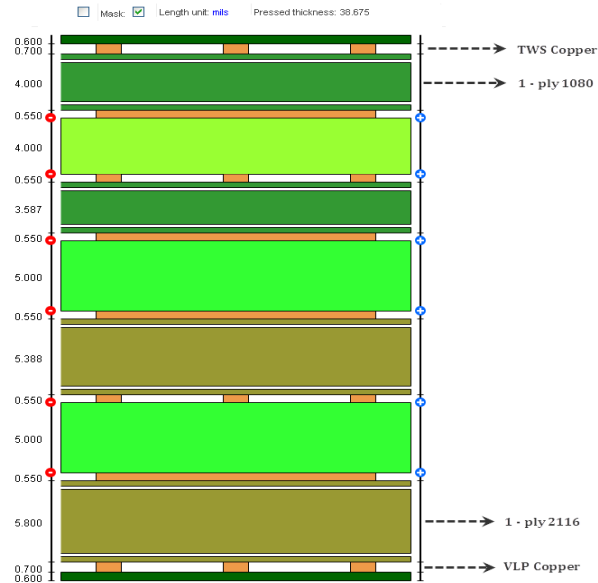


Figure 16: 8-layer stackup of test vehicle.

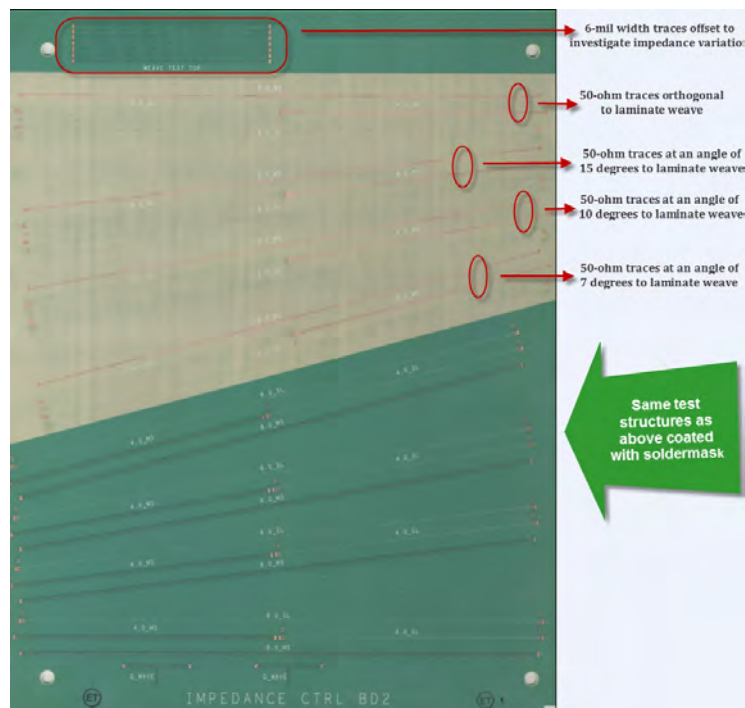


Figure 17: Test vehicle showing the top side structures used for micro-scale effects investigations.

## Experiments

Figure 18 shows that the fabricated lines are terminated with ground-signal-ground (GSG) pads so that coplanar RF-probes with a pitch of  $250\ \mu\text{m}$  can be used to perform  $S$ -parameter measurements. VNA measurements were taken on the following test structures:

- 4 sets of 4-in and 8-in long microstrips coated with OSP with solder mask of 0.6 mils thickness.
- 4 sets of 4-in and 8-in long microstrips coated with OSP without solder mask.
- 2 sets of 3-in long microstrips coated with OSP without solder mask

These measurements were carried out using a vector network analyzer (VNA) which was calibrated up to the probe tips by using a line-reflect-match (LRM) algorithm and an impedance-standard-substrate (ISS) provided by the probe manufacturer. Figure 18 shows the configuration of the measurement setup and a detail of the probing pads that terminate the fabricated microstrips.

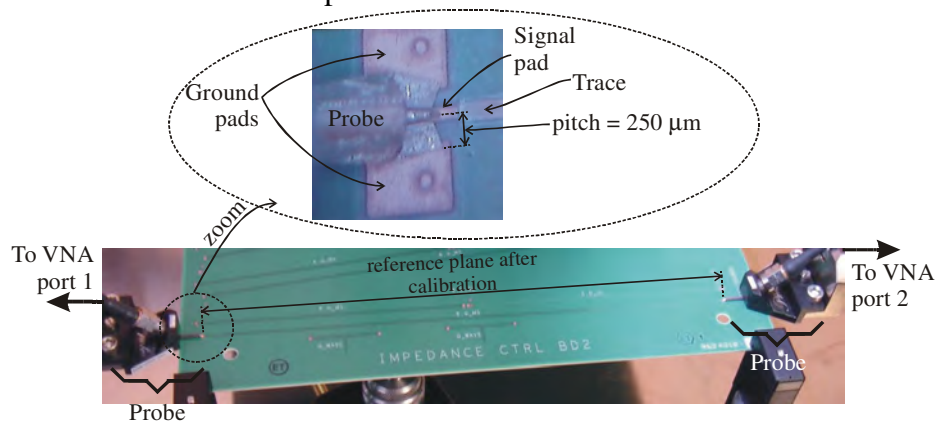


**Figure 18:** Configuration of the measurement equipment.

### Experimental Verification of the Fiber Weave Effect: Resonance

In this section, we perform the experimental verification of the simulation results from the fiber weave section. For that purpose, various microstrip lines were fabricated and measured on the test board previously described. These lines were selected trying to exactly match the structures analyzed by full-wave simulations. That is, 4-in traces running at  $0^\circ$ ,  $5^\circ$ ,  $10^\circ$  and  $15^\circ$  were fabricated and measured for both 1080 and 2116 materials. The results for 1080 are shown in Figure 19.

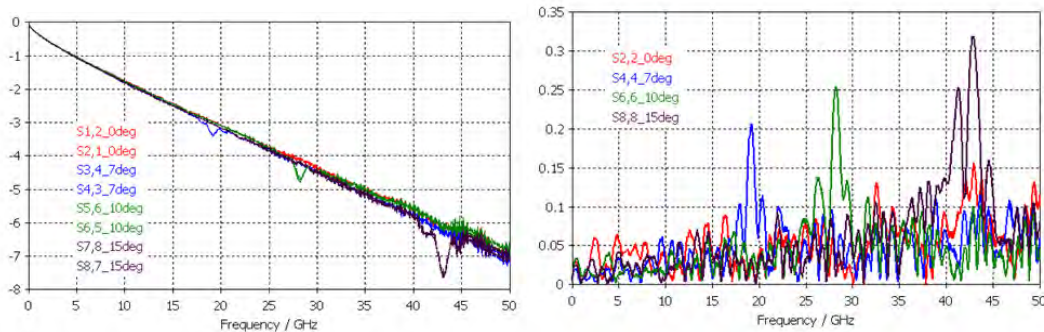


**Figure 19:** Measured results for 4-in traces fabricated on 1080 for  $0^\circ$ ,  $7^\circ$ ,  $10^\circ$  and  $15^\circ$ . *Left:* Insertion loss (dB). *Right:* Return loss (linear scale).

Note that Figure 19 shows the appearance of resonances in the measured data. As expected, the resonance frequencies are in excellent agreement with both, the predictions from the analytical equation and the simulation results from the previous section. Also note that not only the location of the peaks and dips is consistent with the predictions, but also the fact that the magnitude of the resonances increases with the angle as expected.

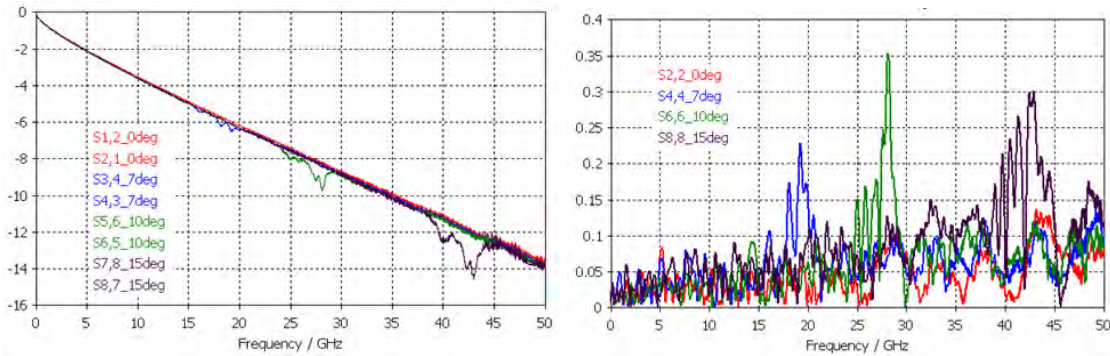


**Figure 20:** Measured results for 8-in traces fabricated on 1080 for  $0^\circ$ ,  $7^\circ$ ,  $10^\circ$  and  $15^\circ$ . *Left:* Insertion loss (dB). *Right:* Return loss (linear scale).

Figure 20 shows the measured results for 8-in traces on 1080 material. Note that the resonances are present as before but they now spread out over a wider frequency range. This is because the fiber weave is not perfect, that is, the weft pitch does not have a constant value but it is also spread around a nominal value. These fiber weave “imperfections” cause the resonance frequency to spread around the predicted resonance frequency. Note that this effect is more noticeable for the 8-in traces than for the 4-in traces. This occurs because the “imperfections” become more noticeable with longer traces because they intersect with the trace more times.

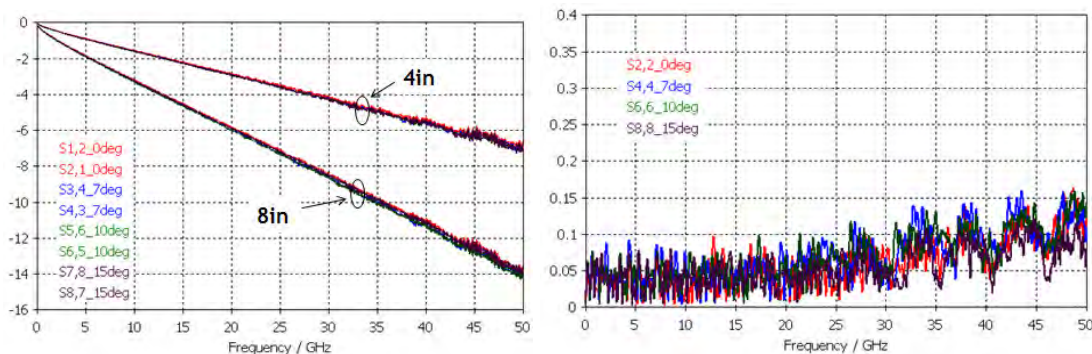


**Figure 21:** Measured results for traces fabricated on 2116 for  $0^\circ$ ,  $7^\circ$ ,  $10^\circ$  and  $15^\circ$ . *Left:* Insertion loss (dB) for 4-in and 8-in. *Right:* Return loss for 8-in (linear scale).

Figure 21 shows the measured results for 4-in and 8-in traces running at different angles fabricated on the 2116 material. The 4-in traces correspond to the simulated structures in the previous section. In contrast to the 1080 case, the results show no resonances in the measured data. As previously discussed, this is a result of the dense weave comprising the 2116 material. Although it is somewhat surprisingly that visible resonances cannot be detected despite our predictions, this is not completely surprising because the idealized

modeling environment tends to overestimate the magnitude of the resonances with respect to measurements [2].

Angle [Deg]	Equation 2 (GHz)	Simulated (GHz)	Measured (GHz)
7°	19.6	19.67	19.17
10°	26.76	27.0	28.2
15°	41.39	41.8	42.86

**Table 4:** Comparison between simulated and predicted resonances for 1080.

### Experimental verification of the fiber weave effect: Position

Afterwards, the propagation constant,  $\gamma$  (per meter) and the characteristic impedance ( $Z_c$ ) were determined from the experimental  $S$ -parameters. These quantities were obtained for inspecting the differences in the electrical properties of lines at different locations on the board, as well as for observing the corresponding variation for lines located at different angles with respect to the fiber wave pattern. In addition, since the board is double-sided and every side presents different glass styles, the characteristics of the microstriplines located on both sides of the PCB are also analyzed. This experiment is carried out to identify additional potential issues (apart from resonances) when using lines with different orientations.

First, the data corresponding to the lines shown in Figure 22 will be discussed. These lines were fabricated on both sides of the PCB, present a length of 3-in, a width of 5.7mils and are separated by 92mils on the 1080 side and 80mils on the 2116 side. For these lines in particular, the characteristic impedance was obtained using the typical ABCD formulation at a frequency so low that the effect of the pad parasitics can be neglected.



**Figure 22:** Microstrips located at different positions within the board.

Figure 23 shows a relatively small variation of the characteristic impedance for the microstrips on both sides of the board.

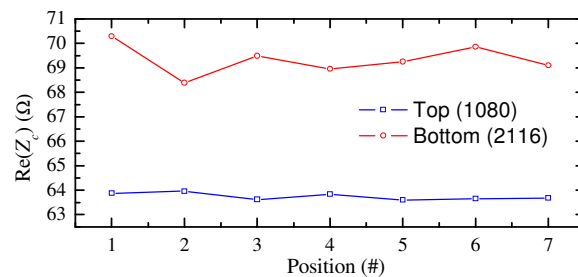


**Figure 23:** Variation of the characteristic impedance with position on both sides of the PCB.

It is important to point out that the variation of the impedances from  $50 \Omega$  in Figure 23 is associated with the fact that narrow lines were used to accentuate the variation of the effective dielectric properties experienced by each line when located at different positions with respect to the weave. However, even in this case the observed changes in  $Z_c$  as a function of position are within the expected variations associated with the tolerances typically specified by the PCB shop ( $\pm 5\%$ ).

A common engineering practice for mitigating the fiber weave effects arising from the position dependence of the traces with respect to the weave, is to introduce an angle between the trace and the fiber weave bundles ( $\Phi \neq 0$ ). In order to assess the effectiveness of this practice, a second experimental analysis was carried out which involves the dependence of the electrical properties of the microstrips with respect to the orientation

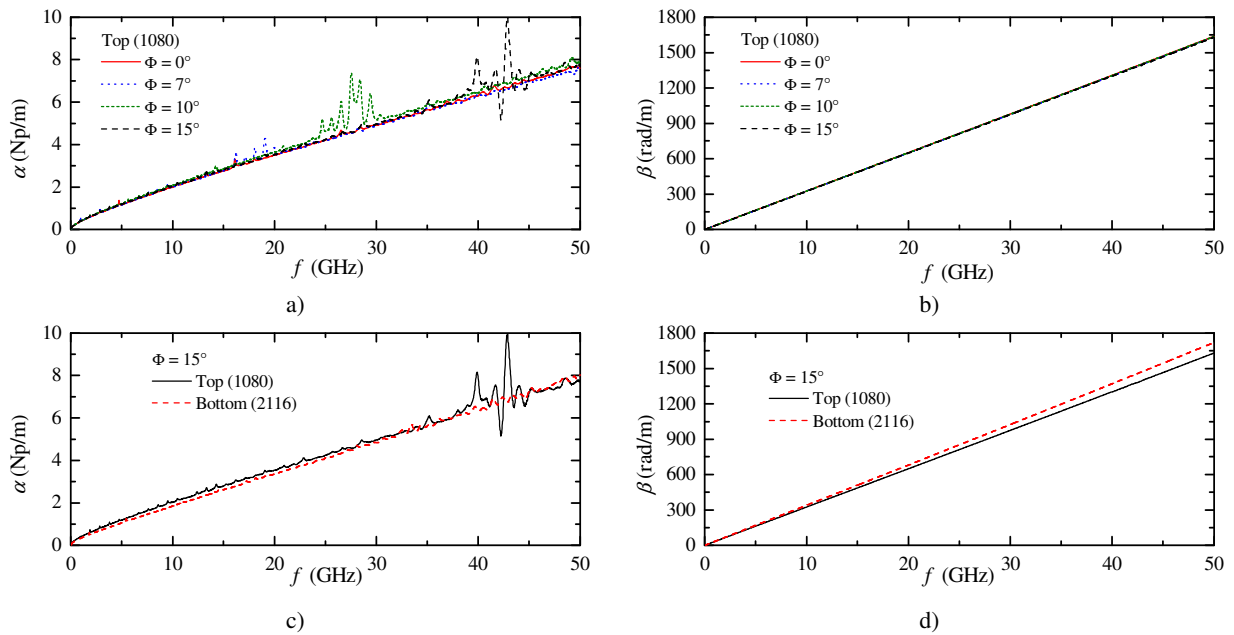


**Figure 24:** Real and imaginary parts of  $\gamma$  as a function of frequency.

(i.e.  $\Phi$ ). For this purpose, since the variation of  $Z_c$  with position for the fabricated microstrips is relatively small as shown in Figure 23, it is reasonable to use a TRL-like line-line de-embedding algorithm [14] to determine  $\gamma = \alpha + j\beta$  as a function of  $\Phi$ . For this purpose, identical pairs of lines varying only in length ( $l = 4$ -in and  $8$ -in) were used for studying every considered angle. The results are shown in Figure 24. Notice that the resonances occurring on the lines fabricated on the 1080 side introduce large fluctuations on the extracted  $\alpha$ , which originate particular bandwidths at which the attenuation presents peaks and the lines act like a reflective device. Notice that, even for  $\Phi = 15^\circ$  this effect is not present in the lines on the 2116 side (Figure 24.c), which is in agreement with the discussions presented above. However, it is worth to mention the difference in  $\beta$  for traces with the same orientation but fabricated on different sides of the PCB (Figure 24.d). This is clearly associated with a change in the effective permittivity due to the different fiber wave patterns of the studied laminates.

On the other hand, notice in Figure 24.b that the resonances are not obvious in the  $\beta$  versus frequency curves for the same group of lines on the 1080 side. This is only because of the large value of the per-unit-length phase delay for the lines. Nonetheless, the resonances become evident when dividing  $\beta$  over  $\omega$ , which is a typical operation used when obtaining  $Z_c$  from the experimental  $\gamma$  [12]. The corresponding curves are shown in Figure 25. These curves also point out a barely noticeable change in the product  $\text{Re}(Z_c)C$  (less than 0.5% in the worst case), which also points out the relatively small variation of  $Z_c$  with  $\Phi$ . This is explicitly illustrated in Figure 26, which shows the extracted characteristic impedance as a function of frequency for different orientations determined using [12]. Again, small variations in this parameter are observed on both sides of the PCB. Thus, notice that even though a critical effect such as that associated with the resonances may occur when changing  $\Phi$ , other not less important parameters such as  $Z_c$  remain relatively low sensitive to this change.

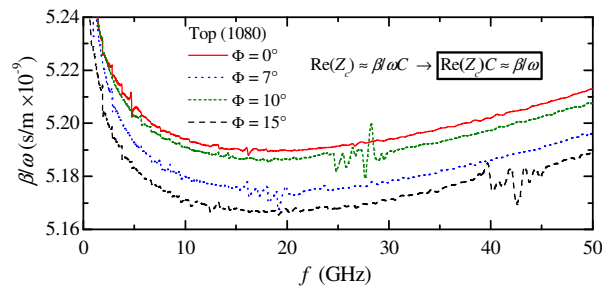


**Figure 25:** Curves illustrating the presence of resonances in the experimentally determined  $\beta$ .

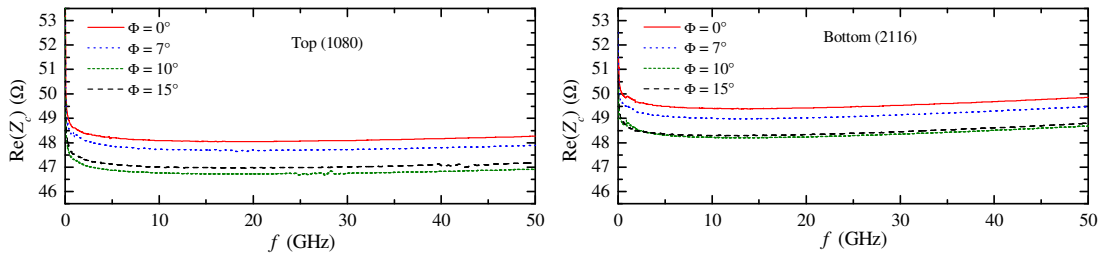


**Figure 26:** Characteristic impedance for microstrips with different orientation for 1080 and 2116.

Finally, the effective relative permittivity was also determined as a function of frequency and  $\Phi$  for lines on both sides of the PCB using a first order approach ( $\epsilon = \beta^2/\omega^2 c^2$ ). The results are shown in Figure 27.

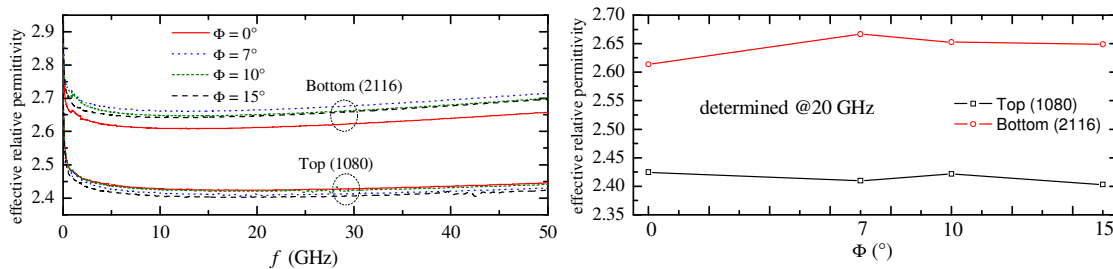


**Figure 27:** Extracted effective permittivity for microstrips on 1080 and 2116 for different angles.

Notice that within the measured frequency range, the maximum variation of  $\epsilon_{eff}$  is less than 2% from trace to trace. This, as well as other discussed results, points out the fact that the more accentuated effect observed in the fabricated structures when changing  $\Phi$  is that associated with the resonances.

From this analysis we can conclude that the engineering practice of rotating the traces with respect to the weave in order to mitigate the fiber weave effect is perfectly safe provided the rotation angle does not lead to resonances. As previously discussed, there are various factors to consider (trace length, glass pitch, fiber weave density), but in general, angles below  $10^\circ$  should be avoided.

### Experimental Verification of the Cu Roughness

As a next step, we use the macroscopic model of surface roughness, which incorporates a surface impedance model, and best known dielectric properties to correlate our simulations to the test vehicle.



Figure 28: Copper “stack-up”.

Figure 28 shows the orientation of the treated and untreated copper sides for the microstrip configuration which corresponds to our prototype. In order to accurately account for the two different sides with different *rms* roughness, we need to split the traces in the middle and assign different materials to the top and the bottom metal parts.

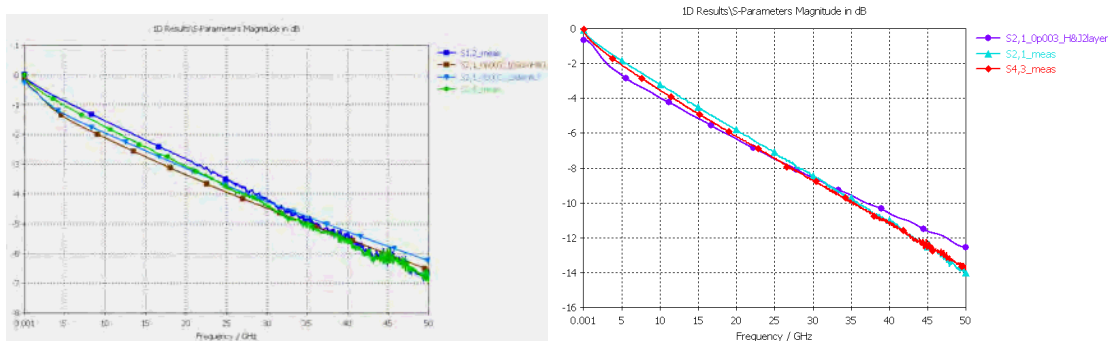


Figure 29: Comparison of simulated versus measured insertion loss: *Left*: 4-in, *Right*: 8-in.

Figure 29 shows the comparison of simulation and measurement. We used a 5<sup>th</sup> order broadband dielectric loss model with the nominal loss tangent of 0.003 [13]. To incorporate the copper losses, we used the aforementioned Hammerstad and Jensen model with the given *rms* roughness datasheet values for the treated and untreated sides.

Simulation and measurement match up to 0.5 dB on the insertion loss using the datasheet values for copper roughness and (constant) dielectric loss. For an even closer match, advanced dielectric and/or roughness models might be needed [14,15].

## **Conclusions**

In this paper, we studied the micro-scale effects of PCB dielectrics in detail. We analyzed the dependence of the electrical properties of interconnects with respect to their position on the weave as well as the effects that result from the periodicity of the fiber glass bundles, which can give rise to resonances. Furthermore, we discussed the mechanisms that produce such resonances and proposed an analytical equation for their prediction, which was validated by 3D electromagnetic simulations and measurements. It should be noted that these results were obtained using a microstrip as a reference and should be extrapolated to striplines with care. In a stripline, the periodicity of the fiber bundles loading the trace is determined by the top and bottom fiber weaves. In particular, the effect of shifted fiber weaves and different glass styles on either side of the stripline should be investigated in more detail. The fiber weave effect in striplines is currently under investigation.

Also, from our investigations we can conclude that the engineering practice of rotating the traces with respect to the weave in order to mitigate the fiber weave effect is perfectly safe provided the rotation angle does not lead to resonances within the desired frequency bandwidth. As previously discussed, there are various factors to consider for proper angle selection (trace length, glass pitch, fiber weave density). Designers should understand the potential effects if they decide to route traces at an angle to the weave.

We have also shown existence of impedance variation as a function of position and angle of the traces with respect to the weave; however, this was shown to be a second order effect of the glass weave. Our test microstrips showed an impedance variation of less than  $2 \Omega$  in range, which correlates to the quasi-flat invariable effective permittivity of the I-Tera material. Although we have not studied the residual skew effect in this paper; our investigations suggest that the resonance caused by periodic loading of the weave fabric adversely affects signal transmission more prominently in high performance dielectric.

For the test vehicle, two different copper finishes were used on the top (1080) and bottom (2116) layers. The experimental data, however, only shows a small difference for the measured microstrip lines. These small differences, combined with the different materials used, made the assessment of contribution to loss from Cu roughness difficult. A more controlled experiment which minimizes the number of variables is underway. By simulation, we showed that surface roughness plays a role in both attenuation as well as signal delay. For the simulation, surface roughness was considered by means of the Hammerstad model. We showed that a surface impedance implementation of this model is quite feasible which supports not only the additional attenuation, but also the increased signal delay. Simulation and measurement match up to 0.5 dB on the insertion loss using the datasheet value for copper roughness and (constant) dielectric loss. For an even closer match, advanced dielectric and/or roughness models might be required.

## References

1. Stephen H. Hall and Howard L. Heck, “*Advanced Signal Integrity for High-Speed Digital Designers*”, Wiley 2009.
2. J. R. Miller, G. J. Blando and I. Novak, “Additional Trace Loss due to Glass-Weave Periodic Loading”, DesignCon 2010, Santa Clara, CA.
3. T. R. Thomas, “*Rough Surfaces*”, Imperial College Press, 2<sup>nd</sup> Ed., 1999.
4. Xiaoxiong Gu, Leung Tsang, Henning Braunsch, “Modeling Effects of Random Rough Interface on Power Absorption Between Dielectric and Conductive Medium in 3-D Problem”, IEEE Trans. MTT, Vol.55, No.3, p511-517, March 2007.
5. E. Hammerstad, O. Jensen, “Accurate Models for Microstrip Computer-Aided Design”, IEEE MTT-S, p.407-409, May 1980.
6. CST STUDIO SUITE™ 2010, [www.cst.com](http://www.cst.com).
7. James C. Rautio, “An Investigation of Microstrip Conductor Loss”, IEEE Microwave Mag.,p.60-67, Dec. 2000.
8. isoStack™ 2010, [www.isola-group.com/isodesign](http://www.isola-group.com/isodesign)
9. Datasheet, *BF-HFI-LP3*, Circuit Foil Luxembourg, available at [www.circuitfoil.com](http://www.circuitfoil.com)
10. Datasheet, TWS, Circuit Foil Luxembourg, available at [www.circuitfoil.com](http://www.circuitfoil.com)
11. J.A. Reynoso-Hernández, “Unified method for determining the complex propagation constant of reflecting and nonreflecting transmission lines,” IEEE Microwave Wireless Comp. Lett., Vol. 13, pp. 351–353, Aug. 2003.
12. R. B. Marks and D. F. Williams, “Characteristic impedance determination using propagation constant measurement,” IEEE Microwave Guided Wave Lett., vol. 1, pp. 141–143, Jun. 1991.
13. M. Schauer, A. Neves, T. Dagostino, S. McMorrow, J. Bell, “Full-wave Time Domain Modeling of Interconnects”, Proceedings of DesignCon 2010.
14. A. F. Horn, J. W. Reynolds, P. A. LaFrance, J. C. Rautio, ”Effect of conductor profile on the insertion loss, phase constant, and dispersion in thin high frequency transmission lines”, Proceedings of DesignCon 2010.
15. A. Koul, P.R. Anmula, M.Y. Koledintseva, J. L. Drewniak, and S. Hinaga, “Improved Technique for Extracting Parameters of Low-Loss Dielectrics on Printed Circuit Boards”, IEEE EMC Symposium. Austin, USA, May 2009.